Microfluid Nanofluid (2010) 9:1125–1133
DOI 10.1007/s10404-010-0633-0

RESEARCH PAPER

Rapid prototyping of PMMA microfluidic chips utilizing a CO_2 laser

Ting-Fu Hong · Wei-Jhong Ju · Ming-Chang Wu · Chang-Hsien Tai · Chien-Hsiung Tsai · Lung-Ming Fu

Received: 18 February 2010 / Accepted: 19 April 2010 / Published online: 26 May 2010

Abstract A commercially available CO_2 laser scriber is used to perform the direct-writing ablation of polymethylmethacrylate (PMMA) substrates for microfluidic applications. The microfluidic designs are created using commercial layout software and are converted into the command signals required to drive the laser scriber in such a way as to reproduce the desired microchannel configuration on the surface of a PMMA substrate. The aspect ratio and surface quality of the ablated microchannels are examined using scanning electron microscopy and atomic force microscopy surface measurement techniques. The results show that a smooth channel wall can be obtained without the need for a post-machining annealing operation by performing the scribing process with the CO_2 laser beam in an unfocused condition. The practicality of the proposed approach is demonstrated by fabricating two microfluidic chips, namely a cytometer, and an integrating microfluidic chip for methanol detection, respectively. The results confirm that the proposed unfocused ablation technique represents a viable solution for the rapid and economic fabrication of a wide variety of PMMA-based microfluidic chips.

Keywords CO_2 laser · Microfluidic chip · PMMA · Unfocused ablation technique

T.-F. Hong · L.-M. Fu (✉)
Department of Materials Engineering, National Pingtung University of Science and Technology, Pingtung 912, Taiwan, ROC
e-mail: loudyfu@mail.npust.edu.tw

W.-J. Ju
Department of Engineering Science, National Cheng Kung University, Tainan 701, Taiwan, ROC

M.-C. Wu
Department of Food Science, National Pingtung University of Science and Technology, Pingtung 912, Taiwan, ROC

C.-H. Tai · C.-H. Tsai (✉)
Department of Vehicle Engineering, National Pingtung University of Science and Technology, Pingtung 912, Taiwan, ROC
e-mail: chtsai@mail.npust.edu.tw

1 Introduction

Microfluidic chips have attracted significant attention over the past decade due to their wide range of potential applications in the biomedical and chemical analysis fields, including capillary electrophoresis (Fu et al. 2007, 2008a; Ohno et al. 2008; Fu et al. 2009), flow cytometry (Fu et al. 2004, 2008b; Tsai et al. 2008; Chen and Wang 2008, 2009; Hou et al. 2009; Lin et al. 2009), polymerase chain reaction (Prakash and Kaler 2007; Prakash et al. 2008; Lund-Olesen et al. 2008; Lien et al. 2009; Allen et al. 2009; Hsieh et al. 2009), DNA amplification (Sundberg et al. 2007; Fu and Lin 2007; Lin et al. 2008), and protein analysis (Choi et al. 2008; Zhang et al. 2008a, b; Lee et al. 2009; Tran et al. 2010). Moreover, many researchers have demonstrated the feasibility of utilizing micromachining techniques to fabricate a network of microchannels on single quartz, glass, or plastic (polymethyl-methacrylate (PMMA), polydimethylsiloxane (PDMS), PC) substrates so as to create microchips capable of performing multiple procedures, e.g., sample handling, mixing, pretreatment, chemical reaction, separation, and so forth (Lee et al. 2006; Lin et al. 2007; Tsai et al. 2007; Beyor et al. 2008; Wu and Li 2008; Fu et al. 2008c; Zhu et al. 2009; Wen et al. 2009; Hairer and Vellekoop 2009; Yeh et al. 2010). Compared to conventional macroscopic devices, microfluidic chips have the

advantages of a reduced solvent, reagent and cell consumption, a more rapid reaction time, a greater portability, a lower cost, and a lower power consumption. In addition, such devices offer the potential for a parallel operation and/or integration with other miniaturized devices to accomplish the lab-on-chip and micro-total-analysis system (μ-TAS).

Most microfluidic devices and master molds are fabricated on silica-based substrates such as glass or quartz. However, these materials require the use of photolithographic and wet chemical etching procedures to pattern the substrate with the required microchannel configuration. From a fabrication point of view, neither technique is ideal since they are relatively time consuming and generate a significant amount of debris. As a consequence, the feasibility of utilizing PMMA substrates for microfluidic applications has attracted increasing interest in recent years. Compared to glass and quartz, PMMA has a number of significant advantages, including a chemical inertness in neutral aqueous solutions and a resistance to hydrolysis. Furthermore, PMMA is a non-porous solid and, therefore, suppresses the contamination effect caused by bimolecular adsorption at the microchannel walls. The literature contains various proposals for the fabrication of PMMA substrates for microfluidic applications, including hot embossing (Liu et al. 2007; Zhang et al. 2008a, b; Juchniewicz et al. 2009), wire imprinting (Martynova et al.1997), and excimer laser ablation (Heng et al. 2006; Qi et al. 2008).

Various groups have investigated the use of laser-based techniques for the patterning of PMMA substrates in recent years. One of the first investigations was performed by Klank et al. (2002), who utilized a CO_2 laser system originally designed for the marking of parts in an industrial setting to scribe microchannels in polymeric substrates. The results showed that microchannels with a depth of 100–300 μm and a width of around 250 μm could be achieved by performing the scribing process using a laser power of 10–60 W and a scanning speed in the range 80–400 mm/s. Liu et al. (2002) fabricated a polycarbonate-based, disposable, monolithic genetic assay device with an integrated PCR, hybridization, and hybridization wash function using a CO_2 laser scribing technique and thermal/adhesive bonding processes. Snakenborg et al. (2004) investigated the feasibility of scribing narrow microchannels on a PMMA surface using a CO_2 laser beam and developed a simple model to relate the channel depth to the velocity, power, and number of passes of the laser system, respectively. In addition, the authors explored the effects of the processing sequence and the number of passes on the cooling time, the channel width, and the channel profile, respectively. Cheng et al. (2004) showed that microfluidic devices with channel aspect ratios ranging from 0.5 to 7 could be accomplished on a single PMMA substrate through a careful control of the CO_2 laser system parameters. In general, the usefulness of the CO_2 laser for the direct writing of PMMA substrates is diminished by the rugged surface of the as-machined trench walls (i.e., 5–10 μm surface roughness) and the limited potential for surface chemistry modification. Nonetheless, Cheng et al. (2004) showed that the fabrication of a channel surface nearly as smooth as pristine PMMA could be achieved without affecting the cross-sectional profile of the channel by performing a one-step thermal annealing treatment after the machining process.

Chung et al. (2005) presented a novel approach for eliminating the characteristic bulge on the rim of CO_2 laser-scribed microchannels in a PMMA substrate by adding an additional layer of PDMS or unexposed photoresist to the polymer substrate prior to the machining process. Wei et al. (2006) utilized a CO_2 laser direct-writing technique to fabricate a microfluidic co-culturing system, which enabled the separation of the two cell types using a microchannel while permitting the transfer of cellular media. Yang et al. (2007) fabricated a microfluidic device by a CO_2 laser machine on a conventional PMMA substrate used a CO_2 laser machine to fabricate a PMMA-based microfluidic device for the encapsulation of ampicillin in chitosan microparticles. The microchip had the advantages of an active control of the droplet diameter (ranging from 100 to 800 μm with a variation of less than 5%), a simple and low-cost fabrication process, and a high throughput. Hsu and Chen (2007) fabricated a diffuser micropump on a PMMA substrate using a CO_2 laser and showed that a maximum flow rate of 14.3 ml/min could be obtained when actuating the membrane with a voltage of 180 V_{PP} at a frequency of 100 Hz. Yuan and Das (2007) presented an experimental and theoretical investigation into the micromachining of PMMA using a CO_2 laser ablation technique. The experimental results showed that microchannels with widths ranging from 44 to 240 μm and depths ranging from 22 to 130 μm could be obtained using a laser power of 0.45–1.35 W and a scanning speed of 2–14 mm/s. Based upon the experimental results, physical models were developed to predict the depth and profile of the ablated channel as a function of the laser processing parameters.

This study develops a high-speed, low-cost CO_2 laser scribing system for the rapid prototyping of PMMA-based microfluidic chips. Compared to existing laser scribing methods, the technique presented in this study utilizes an unfocused laser beam to fabricate the microfluidic channels. The feasibility of the proposed approach is demonstrated by manufacturing two PMMA-based microfluidic chips, namely a self-rotation micro-mixer and a cytometer, respectively. The experimental results confirm that the unfocused laser beam scribing method yields a low microchannel surface roughness in the as-machined condition, and

therefore avoids the need for a post-machining annealing process.

2 Experimental

Figure 1 presents a schematic illustration of the experimental laser machining system used to scribe the PMMA substrates. The CO_2 laser (V-12, Laser Pro Venus, Taiwan) had a maximum output power of 12 W, an output beam diameter of 3.5 mm at the exit, a beam divergence (full angle) of 4 mrad, and a wavelength of 10.6 μm. Moreover, the beam scanning speed was programmable over the range 5–500 mm/s. The laser system was mounted on a 300 × 210 mm^2 *X*–*Y* platform driven by a DC servo control system, while the PMMA substrate was attached to a platform manually adjustable in the *Z*-direction only.

As shown in Fig. 2, scribing trials were performed using two laser beam set-ups, namely a focused laser beam (Fig. 2a) and an unfocused laser beam (Fig. 2b). In the scribing experiments, the laser power was set in the range 1.2–4 W, while the scanning speed was assigned various values between 50 and 150 mm/s. The dimension of the focusing diameter is 0.12 mm. The energy density is 2.55×10^8 W/m^2 for unfocused case ($\lambda = 40$ mm) and 7.08×10^8 W/m^2 for focusing case (using 4 W laser power), respectively. In addition, in the ablation trials performed using the unfocused laser beam, the unfocused height (see Fig. 2b) was set to either 20 or 40 mm by adjusting the position of the *Z*-axis platform accordingly. Following the machining trials, the effects of the laser scribing parameters on the channel depth and surface roughness were evaluated using a scanning electron microscope (SEM, Hitachi S-3000 N, Japan) and a scanning probe microscope (SPM, Veeco CP series, USA). Having determined the optimal machining parameters, the practicality of the laser-writing system was verified by fabricating two microfluidic devices, namely a cytometer, and an integrating microfluidic chip for methanol detection, respectively. The microchannel configurations of the two devices were designed using commercial software, i.e., CorelDraw. The designs were then converted into a sequence of command signals to control the DC servo system used to drive the laser beam in such a way as to reproduce the microchannel designs on a PMMA substrate. The laser system was then used to drill via holes in blank microscope slides with equivalent dimensions to those of the PMMA substrates. Finally, the glass cover plates were fused to the etched PMMA substrates in a thermal bonding process performed for 20 min in a hot embossing machine at a temperature of 105°C and a pressure of 5 kg/cm^2.

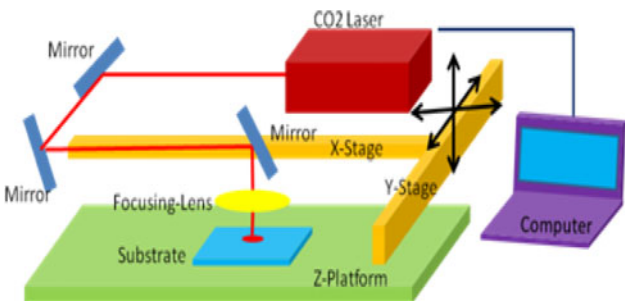

Fig. 1 Configuration of direct-write laser machining system

3 Results and discussions

3.1 Laser scribing of microchannels

Figure 3 shows of direct-write laser machining process performed using focused and unfocused laser beam method for the spot size region and ablation channel shape. The focusing beam method has larger energy density in the direct-writing ablation region (Fig. 3a, focusing method). Therefore, the spot size is smaller and is not easily overlapping in the ablation region. The wave shape and larger rough surface are manufactured in the channel (it is similar, a point manufacture) (Fig. 3b, focusing method). For unfocusing beam method, it has lower energy density in the direct-writing ablation region (Fig. 3a, unfocusing method). The spot size is larger and is easily overlapping in the ablation region (it is similar, a plane manufacture). Therefore, the wave shape can be removed and surface roughness can be improved (Fig. 3b, unfocusing method).

Figure 4a presents an SEM image of a PMMA substrate having three channels of different depths produced using the focused laser beam method with a constant laser power of 4.0 W and scanning speeds of 150, 120, and 80 mm/s, respectively. Note that the PMMA substrate was not annealed after the machining process. It is evident that the channel depth decreases with an increasing scanning speed. However, the aspect ratio is greater than 2:1 in every case. From a qualitative inspection of Fig. 4b, the surface roughness of the microchannel wall was found to exceed 1 μm. Thus, the microchannel is unsuitable for microfluidic applications since a large surface roughness is disadvantageous for chemical or biological analyses.

Figure 5 presents an SEM image of a PMMA substrate with three channels of different depths fabricated using the unfocused laser beam method with a constant scanning power of 4 W, an unfocused height of $\lambda = 20$ mm, and scanning speeds of (a) 80 mm/s, (b) 120 mm/s, and (c) 150 mm/s, respectively. Note that the microchannels were scribed using a single pass of the laser beam. Furthermore, as in the previous example, the substrate was not annealed after the machining process. From inspection, the aspect

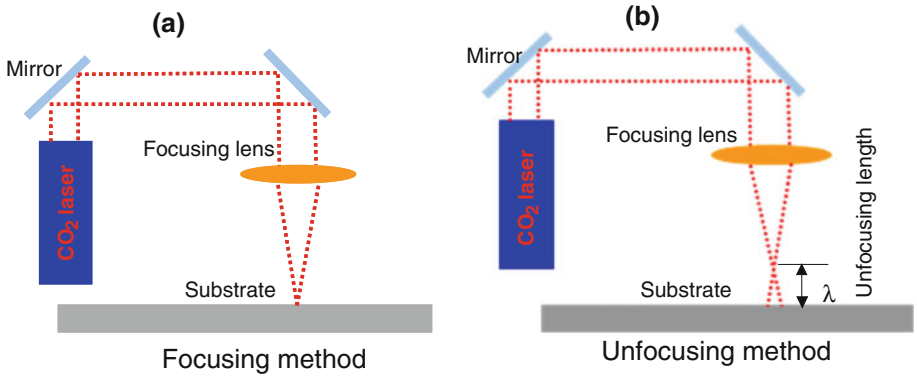

Fig. 2 Schematic illustrations of direct-write laser machining process performed using: **a** focused laser beam method and **b** unfocused laser beam method

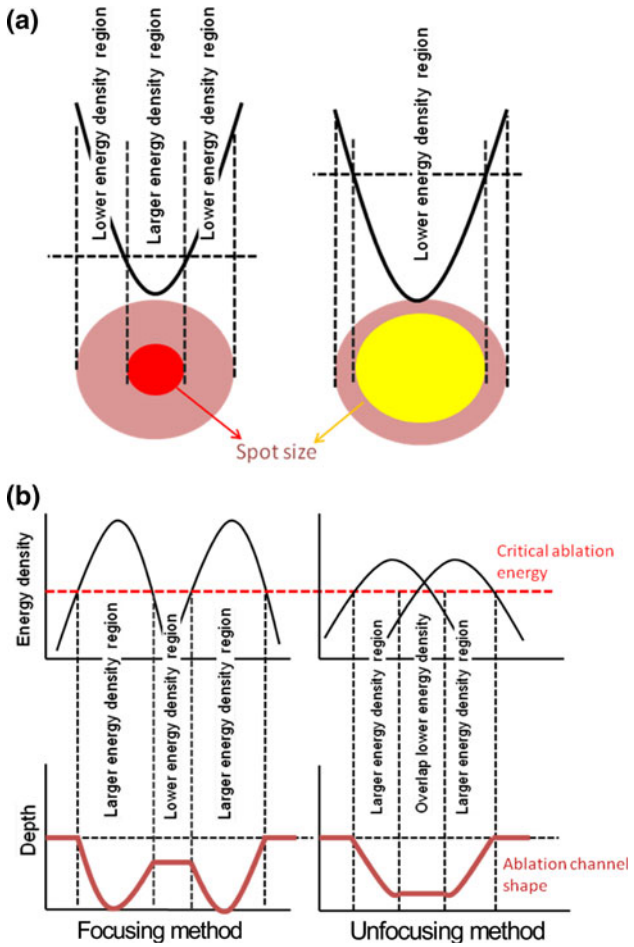

Fig. 3 Schematic illustrations of direct-write laser machining process performed using focused and unfocused laser beam method for the **a** spot size region and **b** ablation channel shape

ratios of the three channels are found to be 2.8, 1.8, and 1.1, respectively. Thus, it is apparent that both the channel depth and the aspect ratio reduce as the scanning speed is increased. Comparing Figs. 4 and 5, it is evident that the unfocused laser beam technique yields a considerable improvement in the surface roughness of the scribed microchannels. However, it can be seen that the surfaces of the microchannels fabricated using the unfocused laser beam technique have a ripple-like characteristic caused by a partial overlap of the laser beam as it is traced over the substrate.

Figure 6 presents an SEM image of a PMMA substrate containing three microchannels of different depths produced using the unfocused laser beam method with a constant scanning speed of 80 mm/s, an unfocused height of $\lambda = 40$ mm, and laser powers of (a) 1.2 W, (b) 2.4 W, (c) 3.6 W, and (d) close-up view of (a) channel bottom, respectively. As in the previous examples, the substrate was not annealed following the machining process. The aspect ratios of the three channels are found to be 1.2, 1.8, and 2.5, respectively. In other words, the aspect ratio increases with an increasing laser power. Furthermore, it can be seen that increasing the unfocused height parameter from $\lambda = 20$ mm to $\lambda = 40$ mm suppresses the ripple-like characteristic on the microchannel surface as a result of the corresponding reduction in the energy density of the laser beam and a comparatively broader etching area. From Fig. 6d, it is shown that the surface roughness of the channel bottom is very well.

Figure 7 presents an atomic force microscopy (AFM) analysis of the surface roughness of a microchannel ablated via the focused laser beam method (Fig. 4b, $\lambda = 0$ mm, 4.0 W, 120 mm/s) and unfocused laser beam method (Fig. 6b, $\lambda = 40$ mm, 2.4 W, 80 mm/s), respectively, without applying a post-processing annealing operation. Note that AFM analysis area is 1 μm × 1 μm. It can be seen that using of the focused beam method yields a relative rougher surface, which average roughness is larger than 2,000 Å, whereas the unfocused laser beam method is capable of achieving a surface roughness of less than 40 Å. It is noted that the surface roughness was obtained by five times of measurement during AFM at different positions. The variation of the measurement is within 10%. The latter result shows the even surfaces, which is therefore suitable for the fabrication of the microchannels within PMMA-based microfluidic devices.

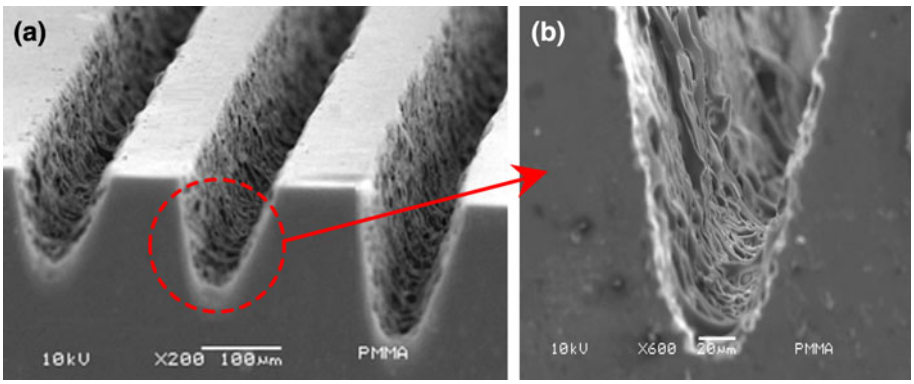

Fig. 4 **a** SEM image of PMMA substrate with channels of different depths produced by focused laser beam with constant laser power of 4.0 W and scanning speeds of 150, 120, and 100 mm/s (for more details, see explanation provided in th text), respectively. **b** Close-up view of ablated microchannel surface (Note that substrate is not annealed following machining process)

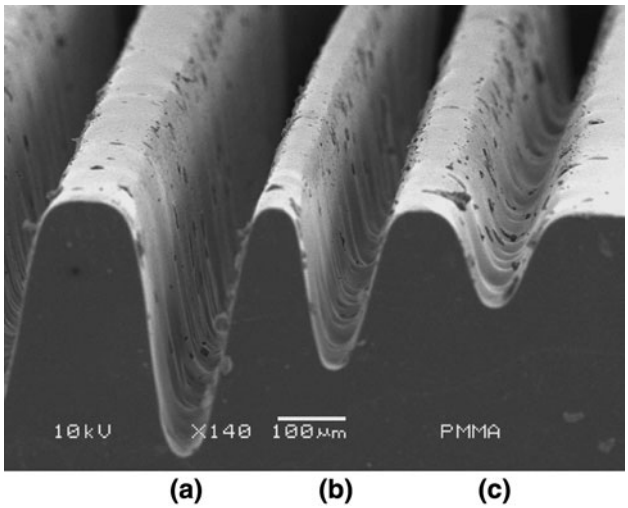

Fig. 5 SEM image of PMMA substrate with channels of different depths produced by unfocused laser beam ($\lambda = 20$ mm) with constant laser power of 4 W and scanning speeds of **a** 80 mm/s, **b** 120 mm/s, and **c** 150 mm/s, respectively (Note that substrate is not annealed following machining process)

3.2 Fabrication of microfluidic chips using unfocused laser beam method

Figure 8 presents two photographs of the microfluidic cytometer fabricated using the unfocused CO_2 laser beam method with a laser power of 1.2 W, an unfocused height of $\lambda = 40$ mm, and a scanning speed of 250 mm/s. The performance of the cytometer was investigated using two water sheath flows and a dye-tinted sample injected into the device under the control of a PC. In the experimental evaluations, focusing ratios (V_2:V_1) ranging from 1:1 to 5:1 were obtained by increasing the sheath flow rate (V_2) from 0.05 to 0.25 µl/min while maintaining the sample flow rate (V_1) at a constant 0.05 µl/min. Figure 9a–c presents experimental images showing the hydrodynamic focusing effect obtained using focusing ratios of 1:1, 2:1, and 5:1, respectively. The images show that the sample stream is successfully constrained by the sheath flows to a narrow region in the center of the microchannel. Figure 9d illustrates the variation of the focused sample stream width with the focusing ratio. Note that the measurement data were acquired at a cross-section located 5 mm downstream from the cytometer nozzle (see Fig. 8b). The results clearly show that the width of the focused sample stream decreases as the focusing ratio increases. Figure 10 presents the optical signals collected by the APD module during an experimental counting test performed using 5-µm fluorescent polystyrene beads and a focusing ratio of 3 (i.e., $V_2 = 0.15$ µl/min and $V_1 = 0.05$ µl/min). The results confirm that the micro-particles in the sample stream can be focused and detected by the proposed device successfully.

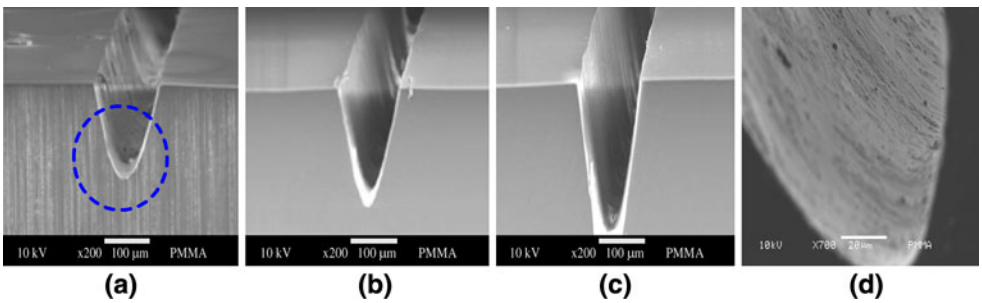

Fig. 6 SEM images of PMMA substrate with channels of different depths produced by unfocused laser beam method ($\lambda = 40$ mm) with constant scanning speed of 80 mm/s and laser powers of **a** 1.2 W, **b** 2.4 W, **c** 3.6 W, and **d** close-up view of **a** channel bottom, respectively. (Note that substrate is not annealed following machining process)

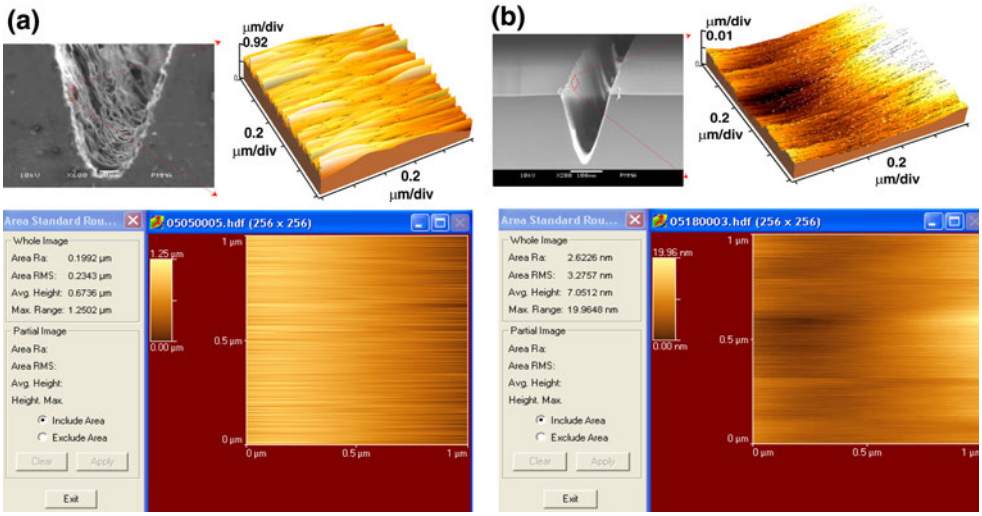

Fig. 7 AFM scanning results showing surface roughness of microchannel produced using **a** focused laser beam method ($\lambda = 0$ mm, 4.0 W, 120 mm/s), and **b** unfocused laser beam method ($\lambda = 40$ mm, 2.4 W, 80 mm/s)

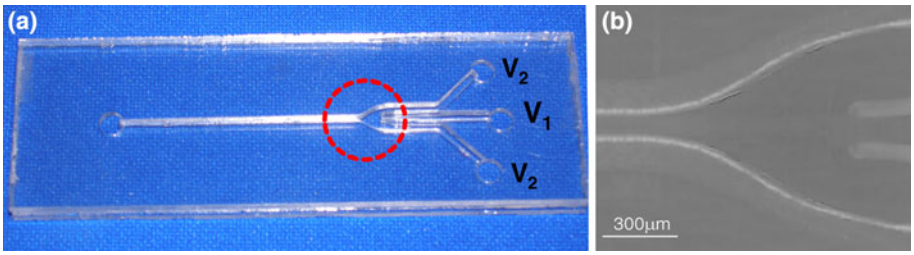

Fig. 8 **a** Photograph of micro-cytometer fabricated using laser scribing method. **b** Close-up view of micro-nozzle in micro-cytometer

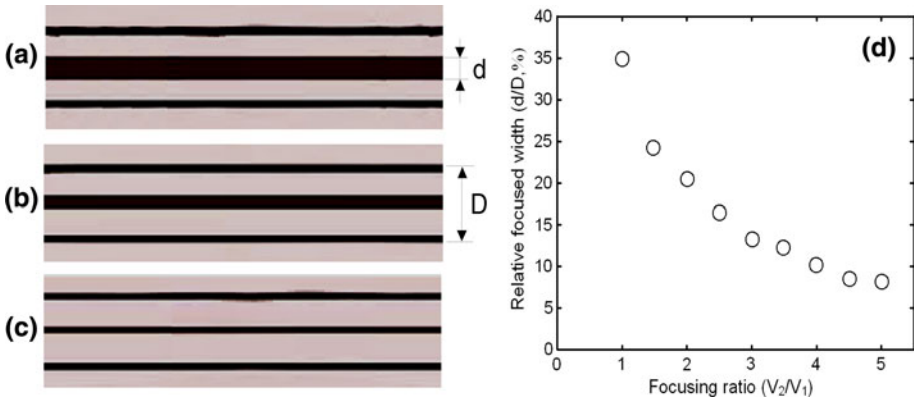

Fig. 9 Experimental results for sample stream distribution obtained using focusing ratios (V_2/V_1) of: **a** $V_2/V_1 = 1$, **b** $V_2/V_1 = 2$, **c** $V_2/V_1 = 5$, and **d** variation of focused stream width with focusing ratio

Figure 11 presents a photograph of the current microfluidic device designed to perform rapid methanol detection system. Note that the microchannels was fabricated by the unfocused CO_2 laser beam method with a laser power of 1.2 W, an unfocused height of $\lambda = 40$ mm, and a scanning speed of 250 mm/s. The device measures 5 cm × 2.5 cm and incorporates two mixing chambers and two serpentine reaction channels of dimensions 150 μm × 60 μm (width × depth) for methanol detection. The detection method is called Schiff method (Klavons and Bennett 1986). The rapid methanol detection system comprises first mixing column for the mixture of MOX (methanol oxidase) and methanol, first reaction column for the reaction of MOX–methanol to the formaldehyde, secondary mixing column for the mixture of formaldehyde and basic fuchsin, and secondary reaction column for detecting of sample collection by the formaldehyde–basic fuchisn reaction. In the meanwhile, the temperature of the formaldehyde–basic fuchisn reaction column was maintained at a constant 35°C using a TE (Thermoelectric) cooler. The final methanol reactant products obtained from the proposed microchip and the methanol reactant produced from a standard tube system analyzed their optical density (OD) value simultaneously using a conventional UV spectrophotometer.

Figure 12 presents a series of experimental images showing the evolution of the flow rotation effect within the

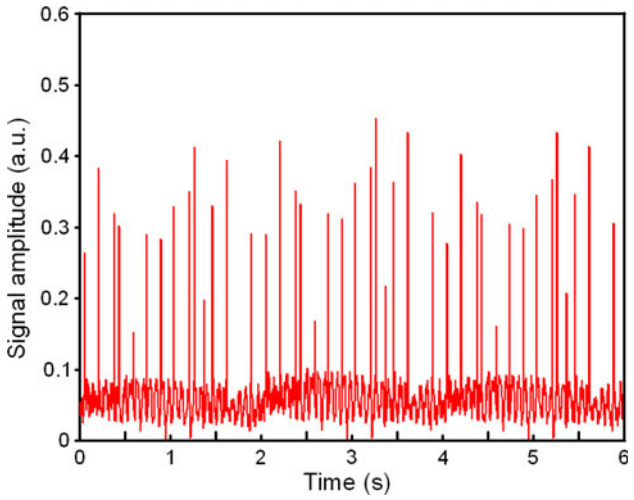

Fig. 10 Optical signals collected by APD module with counting 5-μm fluorescent polystyrene beads

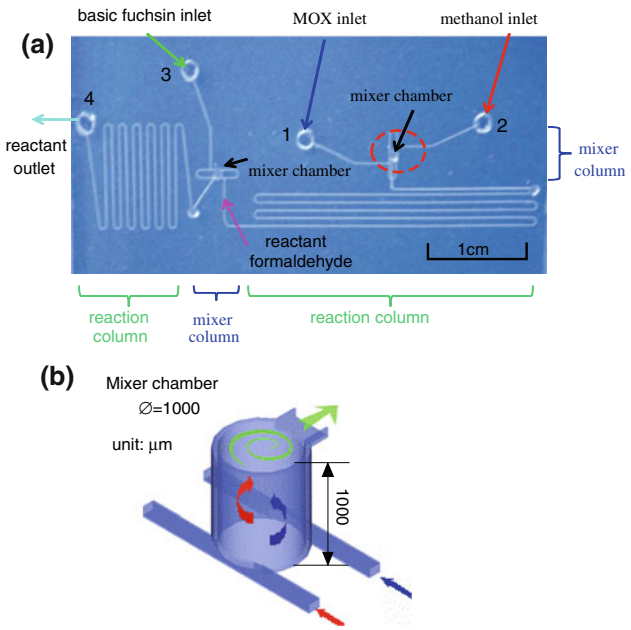

Fig. 11 **a** Photograph of methanol detection microfluidic system fabricated using laser scribing method, and **b** schematic illustration of micro-chamber geometry

circular microchamber when Rhodamine B fluorescent dye was injected into the micro-mixer with a Reynolds number of $Re = 4$. Note that detailed descriptions of the mixing effect and mixing mechanisms in circular microfluidic mixers have been presented previously by the current authors (Lin et al. 2005, 2007). The images show that when the fluorescent die and buffer solution are initially loaded into the microchamber, the species concentration distribution exhibits two distinct regions. However, the driving force is sufficient to establish a rotational flow effect in the

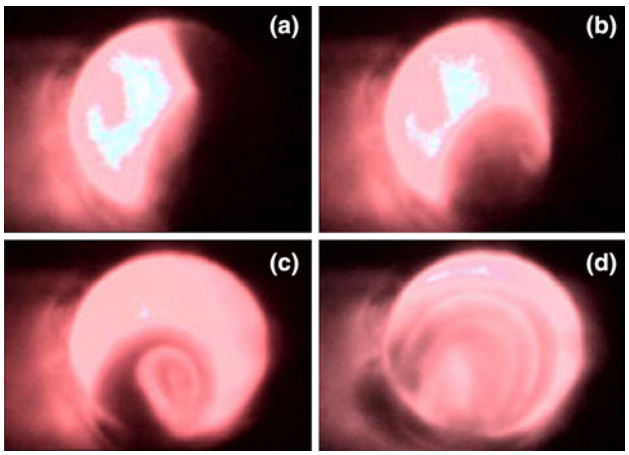

Fig. 12 Experimental images showing flow rotation effect induced in micro-chamber of micro-mixer at $Re = 4$ after: **a** 2, **b** 4, **c** 7, and **d** 10 s

microchamber, and thus a 3-D vortex is formed within 10 s (see Fig. 12d). Analyzing the results of outlet region, it is found that a mixing ratio of 95.8% is obtained for a Reynolds number of $Re = 4$. The result confirms that the sample and reagent can be mixed efficaciously and rapidly by the circular microfluidic mixer in this methanol detection system.

Figure 13 presents the optimized operating conditions for the proposed methanol detection system under different unit of MOX with corresponding reaction time. The result indicates that a higher unit MOX (see 2 unit MOX) can result in a faster reaction (reaction time about 10 min) and also a suitable OD (OD value larger than 0.265) for the

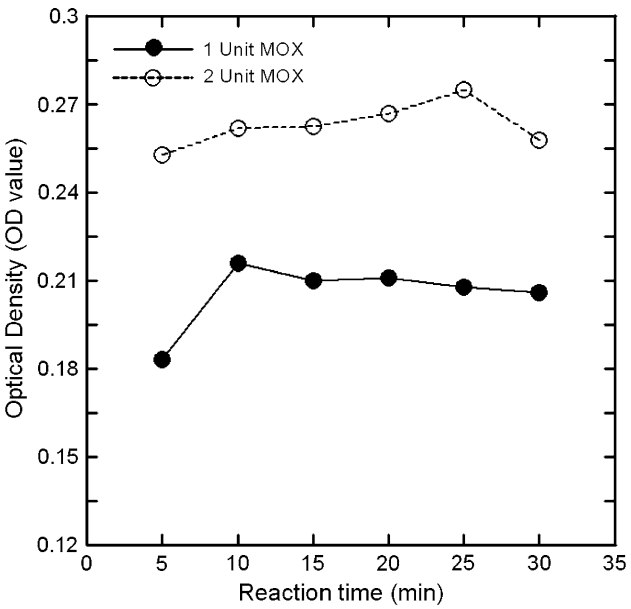

Fig. 13 Relationships between the minimum time required for different unit of MOX with corresponding reaction time

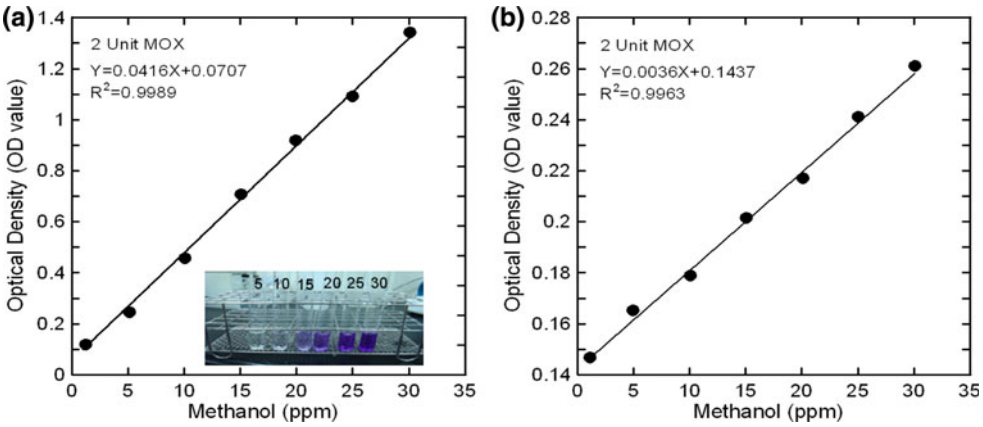

Fig. 14 The OD value of methanol detection results for **a** a conventional tube system and **b** an integrating microfluidic system

MOX–methanol reaction. Figure 14a presents the detected methanol concentration results using of a traditional large-scale system. By means of the traditional large-scale system, 1 ml of methanol and 1 ml MOX were mixed in the tube and maintained at a constant 25°C about 30 min. The basic fuchisn and HCl were then increased in the tube and maintained at a constant 35°C about 2 h. The final methanol reactant products were corrected from the tube and used a conventional UV spectrophotometer to detect the OD value. The R square and relation are found to be $R^2 = 0.9989$ and $Y = 0.0416X + 0.0707$. Figure 14b presents the detected methanol concentration results using the present integrating microfluidic system. By means of the proposed microfluidic system, 0.15 ml of methanol (inlet 1) and 0.15 ml MOX (inlet 2) were mixed in first micromixer chamber. The MOX–methanol reacted with the formaldehyde through the first reaction column and maintained at a constant 25°C about 15 min. The basic fuchisn and HCl were then injected from inlet 4 port through the secondary reaction column and maintained at a constant 35°C using a TE (Thermoelectric) cooler about 15 min. The final methanol reactant products were corrected from the outlet port (port 4) and their OD value was detected by a conventional UV spectrophotometer. The R square and relation are found to be $R^2 = 0.9963$ and $Y = 0.0036X + 0.1437$. In this case, a rapid and thorough mixing was achieved in the mixing and reaction column for the proposed microfluidic chip, such that only 30 min of reaction time was enough to complete the methanol detection.

4 Conclusions

This article has presented a novel technique for scribing microchannels in PMMA substrates using a continuous-wave unfocused CO_2 laser beam. The SEM and AFM results have shown that a microchannel surface roughness of less than 40 Å can be obtained without the need for a post-machining annealing process by utilizing a laser power of 2.4 W, an unfocused height of $\lambda = 40$ mm, and a scanning speed of 80 mm/s. The practicality of the proposed unfocused laser beam machining process has been demonstrated by fabricating a capillary electrophoresis microchip, a cytometer, and an integrating microfluidic chip. Overall, the experimental results have confirmed that the proposed technique represents a low-cost and versatile solution for the rapid prototyping of PMMA-based microfluidic devices.

Acknowledgments The authors gratefully acknowledge the financial support provided to this study by the National Science Council of Taiwan under Grant NSC97-2320-B-020-001-MY3 and NSC98-2113-M-020-001.

References

Allen JW, Kenward M, Dorfman KD (2009) Coupled flow and reaction during natural convection PCR. Microfluid Nanofluid 6:121–130

Beyor N, Seo TS, Liu P, Mathies RA (2008) Immunomagnetic bead-based cell concentration microdevice for dilute pathogen detection. Biomed Microdevices 10:909–917

Chen HT, Wang YN (2008) Fluorescence detection in a micro flow cytometer without on-chip fibers. Microfluid Nanofluid 5: 689–694

Chen HT, Wang YN (2009) Optical microflow cytometer for particle counting, sizing and fluorescence detection. Microfluid Nanofluid 6:529–537

Cheng JY, Wei CW, Hsu KH, Young TH (2004) Direct-write laser micromachining and universal surface modification of PMMA for device development. Sens Actuators B Chem 99:186–196

Choi D, Jang E, Park J, Koh W (2008) Development of microfluidic devices incorporating non-spherical hydrogel microparticles for protein-based bioassay. Microfluid Nanofluid 5:703–710

Chung CK, Lin YC, Huang GR (2005) Bulge formation and improvement of the polymer in CO_2 laser micromachining. J Micromech Microeng 15:1878–1884

Fu LM, Lin CH (2007) A rapid DNA digestion system. Biomed Microdevices 9:277–286

Fu LM, Yang RJ, Lin CH, Lee GB, Pan YJ (2004) Electrokinetically driven micro flow cytometers with integrated fiber optics for on-line cell/particle detection. Anal Chim Acta 507:163–169

Fu LM, Leong JC, Lin CF, Tai CH, Tsai CH (2007) High performance microfluidic capillary electrophoresis devices. Biomed Microdevices 9:405–412

Fu LM, Lee CY, Liao MH, Lin CH (2008a) Fabrication and testing of high-performance detection sensor for capillary electrophoresis microchips. Biomed Microdevices 10:73–80

Fu LM, Tsai CH, Lin CH (2008b) A high-discernment microflow cytometer with microweir structure. Electrophoresis 29: 1874–1878

Fu LM, Hong TF, Wen CY, Tsai CH, Lin CH (2008c) Electrokinetic instability effects in microchannels with and without nanofilm coatings. Electrophoresis 29:4871–4879

Fu LM, Wang JH, Luo WB, Lin CH (2009) Experimental and numerical investigation into the joule heating effect for electrokinetically driven microfluidic chips utilizing total internal reflection fluorescence microscopy. Microfluid Nanofluid 6: 499–507

Hairer G, Vellekoop MJ (2009) An integrated flow-cell for full sample stream control. Microfluid Nanofluid 7:647–658

Heng Q, Tao C, Zho T (2006) Surface roughness analysis and improvement of micro-fluidic channel with excimer laser. Microfluid Nanofluid 2:357–360

Hou HH, Tsai CH, Fu LM, Yang RJ (2009) Experimental and numerical investigation into micro-flow cytometer with 3-D hydrodynamic focusing effect and microweir structure. Electrophoresis 30:2507–2515

Hsieh TM, Luo CH, Wang JH, Lin JL, Lien KY, Lee GB (2009) A two-dimensional, self-compensated, microthermal cycler for one-step reverse transcription polymerase chain reaction applications. Microfluid Nanofluid 2:357–360

Hsu YC, Chen TY (2007) Applying Taguchi methods for solvent-assisted PMMA bonding technique for static and dynamic μ-TAS devices. Biomed Microdevices 9:513–522

Juchniewicz M, Chudy M, Brzózka Z, Dybko A (2009) Bonding-less (B-less) fabrication of polymeric microsystems. Microfluid Nanofluid 7:733–737

Klank H, Kutter JP, Geschke O (2002) CO_2-laser micromachining and back-end processing for rapid production of PMMA-based microfluidic systems. Lab Chip 2:242–247

Klavons JA, Bennett RD (1986) Determination of methanol using alcohol oxidase and its application to methylester content of pectins. J Agric Food Chem 34:597–605

Lee CY, Chen CM, Chang GL, Lin CH, Fu LM (2006) Fabrication and characterization of semicircular detection electrodes for contactless conductivity detector–CE microchips. Electrophoresis 27:043–5050

Lee CY, Lin YH, Lee GB (2009) A droplet-based microfluidic system capable of droplet formation and manipulation. Microfluid Nanofluid 6:599–610

Lien KY, Lee SH, Tsai TJ, Chen TY, Lee GB (2009) A microfluidic-based system using reverse transcription polymerase chain reactions for rapid detection of aquaculture diseases. Microfluid Nanofluid 7:795–806

Lin CH, Tsai CH, Fu LM (2005) A rapid 3-dimensional vortex micromixer utilizing self-rotation effect under low Reynolds number conditions. J Micromech Microeng 15:935–943

Lin CH, Tsai CH, Fu LM (2007) Rapid circular microfluidic mixer utilizing unbalanced driving force. Biomed Microdevices 9: 43–50

Lin CH, Wang JH, Fu LM (2008) Improving the separation efficiency of DNA biosamples in capillary electrophoresis microchips using high-voltage pulsed DC electric fields. Microfluid Nanofluid 5:403–410

Lin CH, Lee CY, Tsai CH, Fu LM (2009) Novel continuous particle sorting in microfluidic chip utilizing cascaded squeeze effect. Microfluid Nanofluid 7:499–508

Liu Y, Rauch CB, Stevens RL, Lenigk R, Yang J, Rhine DB, Grozinski P (2002) DNA amplification and hybridization assays in integrated plastic monolithic devices. Anal Chem 74:3063–3070

Liu Y, Cady NC, Batt CA (2007) A plastic microchip for nucleic acid purification. Biomed Microdevices 9:769–776

Lund-Olesen T, Dufva M, Dahl JA, Collas P, Hansen MF (2008) Sensitive on-chip quantitative real-time PCR performed on an adaptable and robust platform. Biomed Microdevices 10:769–776

Martynova L, Locascio LE, Gaitan M, Kramer GW, Christensen RG, MacCrehan WA (1997) Fabrication of plastic microfluid channels by imprinting methods. Anal Chem 69:4783–4789

Ohno K, Tachikawa K, Manz A (2008) Microfluidics: applications for analytical purposes in chemistry and biochemistry. Electrophoresis 29:4443–4453

Prakash R, Kaler KVIS (2007) An integrated genetic analysis microfluidic platform with valves and a PCR chip reusability method to avoid contamination. Microfluid Nanofluid 3:177–187

Prakash R, De la Rosa C, Fox JD, Kaler KVIS (2008) Characteristics and impact of *Taq* enzyme adsorption on surfaces in microfluidic devices. Microfluid Nanofluid 4:451–456

Qi H, Chen T, Yao L, Zuo T (2008) Hydrophilicity modification of poly(methyl methacrylate) by excimer laser ablation and irradiation. Microfluid Nanofluid 5:139–143

Snakenborg D, Klank H, Kutter JP (2004) Microstructure fabrication with a CO_2 laser system. J Micromech Microeng 14:182–189

Sundberg SO, Wittwer CT, Greer J, Pryor RJ, Elenitoba-Johnson O, Gale BK (2007) Solution-phase DNA mutation scanning and SNP genotyping by nanoliter melting analysis. Biomed Microdevices 9:159–166

Tran NT, Ayed I, Pallandre A, Taverna M (2010) Recent innovations in protein separation on microchips by electrophoretic methods: an update. Electrophoresis 31:147–173

Tsai CH, Chen HT, Wang YN, Lin CH, Fu LM (2007) Capabilities and limitations of 2-dimensional and 3-dimensional numerical methods in modeling the fluid flow in sudden expansion microchannels. Microfluid Nanofluid 3:13–18

Tsai CH, Hou HH, Fu LM (2008) An optimal three-dimensional focusing technique for micro-flow cytometers. Microfluid Nanofluid 5:827–836

Wei CW, Cheng JY, Young TH (2006) Elucidating in vitro cell-cell interaction using a microfluidic coculture system. Biomed Microdevices 8:65–71

Wen CY, Yeh CP, Tsai CH, Fu LM (2009) Rapid magnetic microfluidic mixer utilizing AC electromagnetic field. Electrophoresis 30:4179–4186

Wu Z, Li D (2008) Mixing and flow regulating by induced-charge electrokinetic flow in a microchannel with a pair of conducting triangle hurdles. Microfluid Nanofluid 5:67–76

Yang CH, Huang KS, Chang JY (2007) Manufacturing monodisperse chitosan microparticles containing ampicillin using a microchannel chip. Biomed Microdevices 9:253–259

Yeh CH, Lin PW, Lin YH (2010) Chitosan microfiber fabrication using a microfluidic chip and its application to cell cultures. Microfluid Nanofluid 8:115–121

Yuan D, Das S (2007) Experimental and theoretical analysis of direct-write laser micromachining of polymethyl methacrylate by CO_2 laser ablation. J Appl Phys 101:024901

Zhang L, Gu F, Tong L, Yin X (2008a) Simple and cost-effective fabrication of two-dimensional plastic nanochannels from silica nanowire templates. Microfluid Nanofluid 5:727–732

Zhang J, Das C, Fan ZH (2008b) Dynamic coating for protein separation in cyclic olefin copolymer microfluidic devices. Microfluid Nanofluid 5:327–335

Zhu J, Tzeng TJ, Hu G, Xuan X (2009) DC dielectrophoretic focusing of particles in a serpentine microchannel. Microfluid Nanofluid 7:751–756